Chemical Engineering Journal 251 (2014) 1–9

Contents lists available at ScienceDirect

Chemical Engineering Journal

journal homepage: www.elsevier.com/locate/cej

Swelling-agent-free synthesis of rice husk derived silica materials with large mesopores for efficient CO_2 capture

Wanting Zeng, Hsunling Bai *

Institute of Environmental Engineering, National Chiao Tung University, 1001 University Rd., Hsinchu 300, Taiwan

HIGHLIGHTS

- Biporous MS-400(25) with large mesopores was prepared without swelling agents.
- Using silicate waste of rice husk as precursor reduces the chemical costs.
- MS-400(25) made from agricultural waste can be a potential CO_2 adsorbent.

ARTICLE INFO

Article history:
Received 3 March 2014
Received in revised form 7 April 2014
Accepted 10 April 2014
Available online 24 April 2014

Keywords:
Rice husk ash (RHA)
Waste resource recovery
Mesoporous silica material
CO_2 adsorption
Carbon dioxide capture

ABSTRACT

Swelling-agent-free synthesis of silica materials with large mesopores were developed using silicate from rice husk ash (RHA) as an alternative silica precursor in this study. Unlike the conventional methods for preparing large-pore silica materials in which toxic and expensive additives were employed as swelling agents, the obtained silica materials with large mesopores could be facilely prepared via a simple temperature-controlled approach without adding pore expanders. The fusion and hydrothermal temperature effects on the structural properties of obtained mesoporous silicas were investigated by the XRD, nitrogen adsorption–desorption, SEM and TEM analyses. The obtained mesoporous MS-400(25), which was fabricated using rice husk fused at 400 °C and treated with sodium hydroxide at 25 °C, exhibited bimodal meso-porosities (2.7 and 24 nm) and large pore volume (1.92 cm^3/g). The bi-porosities mainly originated from the intra-particle mesostructure within silica particles and the inter-particle porosity between the aggregated nano-sized silica particles, respectively. The synthesized silicas were applied as the supports of adsorbents for CO_2 capture. The adsorption tests clearly revealed that the tetraethylenepentamine (TEPA) impregnated MS-400(25) material could achieve CO_2 adsorption capacity of 173 mg/g under 10% CO_2 at 75 °C, which was the best sorbents among all samples due to its relatively large pore volume.

1. Introduction

The mitigation of global warming due to CO_2 emission is of great importance in environmental protection. Among available technologies, the use of amine-based solid sorbents for controlling CO_2 emission has attracted considerable attention, particularly in post-combustion processes where CO_2 is captured at low temperature and low pressure [1–4]. In comparison with conventional amine-based solvent scrubbing, the use of solid sorbents shows great potential to reduce the cost of capture process and lessen the energy penalty [5,6]. Therefore, the development of efficient and low-cost CO_2 sorbents will undoubtedly enhance the competitiveness for CO_2 capture applications [7,8].

Recently mesoporous silicas with tunable pore texture and unique surface chemistry via functionalization are considered as promising adsorbents for CO_2 capture [9]. Progress has been made by functionalizing various amine-based polymers on several supports including MCM-41, SBA-15, HMS, KIT, MSU, mesoporous silica spherical particles and mesocellular foams [10–16]. And high sorbent capacity and selectivity have been achieved for CO_2 capture. More recently, research works have shown that the pore size and pore volume of silica support play important roles in sorbent performance [17–19]. Supports with high pore volume can accommodate a greater amount of amines in the pores, and a large pore size is desirable for rapid diffusion of CO_2 in the pores. In this regard, mesocellular foams and mesoporous silica with large pore size and good pore interconnection appear to be more efficient than the other mesoporous silica supports [19–21].

Silicon alkoxide and sodium silicate are common silica sources [22,23]. However, the commercial fabrications of silica sources are

* Corresponding author. Tel.: +886 3 5731868; fax: +886 3 5725958.
E-mail address: hlbai@mail.nctu.edu.tw (H. Bai).

http://dx.doi.org/10.1016/j.cej.2014.04.041
1385-8947/

highly energy-consumed and associated with high temperature, high pressure and strong acidity process [24,25], which is expensive and unfriendly to the environment. In addition, in the preparation of silica supports with large pores and hierarchical structures for efficient CO_2 capture, the use of toxic and expensive swelling agents such as trimethylbenzene (TMB) and ammonium fluoride are required [26,27]. Thus the industrial applications of current methods would have certain limitations in terms of environment, energy and economic concerns.

The recycling of silicon or silica-containing wastes as alternative precursors for preparing mesoporous silica instead of using commercial agents may provide an excellent opportunity to prepare the sorbents economically and minimize the waste production as well. Rice husk (RH) is one of the major agricultural wastes around the world, and it has been demonstrated to be a potentially feasible resource for synthesizing silica-based materials [28–30]. With the aim of lowering manufacturing cost and green synthesis for CO_2 adsorbent, a series of polyethyleneimine-immobilized uni-modal and/or bi-modal porous silicas were prepared from rice husk ash with biopolymer of chitosan as a pore structure-directing agent [31]. However, the maximum pore volume of their prepared silica support was only 1.08 cm^3/g, which could only accommodate ca. 50 wt.% amines. From the viewpoint of both lowering cost and green synthesis, it is highly desirable to develop a simple and scalable approach to prepare silica supports with large pore volume and large pore size.

In this study, the fabrication of mesoporous silica materials with different mesopore sizes and large pore volumes were prepared by using sodium silicate solution as silica source via a simple temperature-controlled approach. The sodium silicate solution, which is extracted from rice husk ash (RHA), has been demonstrated to be a potentially feasible resource for synthesizing silica-based materials. The synthetic process is simple, cost-effective and environmentally benign since no extra pore expander and post-pore-expansion treatment are necessary, which significantly simplifies the scale-up synthesis. The pore structure and morphology of the obtained silica materials are presented and discussed. Moreover, an attempt has also been made to apply these mesoporous silica for immobilization of tetraethylpentaamine (TEPA) as sorbents and investigate their structure vs. performance relationship for CO_2 capture.

2. Experimental section

2.1. Silica extraction and material preparation

In order to figure out the effect of fusion temperature on structural properties of the obtained MS materials, the rice husk (RH) was fused under 400, 550 or 700 °C, respectively, and the obtained rice husk ash (RHA) was then mixed with aqueous NaOH solution at 25 °C for 24 h for the extraction of silica. The resulting mixture was then centrifuged to separate supernatant and sediment. The silicate supernatant was then utilized as the silica precursor for the synthesis of mesoporous silica materials. Mesoporous silicas were synthesized by the hydrothermal treatment method using the silicate supernatant extracted from RHA as the silica precursor and cetyltrimethylammonium bromide (CTAB) was employed as the structure-directing template in the synthesis. The molar composition of the gel mixture was 1 SiO_2: 0.2 CTAB: 0.89 H_2SO_4: 120 H_2O. In a typical procedure, 63 ml of waste silicate solution was acidified by adding approximately 40 ml of 4N H_2SO_4 to bring down the pH to 10.5 with constant stirring to form a gel. After stirring, 7.28 g of CTAB (dissolved in 25 ml of DI water) was added drop by drop into the above mixture and the combined mixture was stirred for three additional hours. The resulting gel mixture was transferred into a Teflon coated autoclave and kept in an oven at 145 °C for 36 h. After cooling to room temperature, the resultant solid was recovered by filtration, washed with DI water and dried in an oven at 110 °C for 8 h. Finally, the organic template was removed by using a muffle furnace in air at 550 °C for 6 h. The synthesized mesoporous silica was denoted as MS-X(25), where X corresponds to the fusion temperature of raw RH under 400, 550 or 700 °C, with the following silica extraction temperature at 25 °C.

On the other hand, for studying the effect of extraction temperature on structural properties of the obtained MS materials, the RH was fused under a fixed temperature of 400 °C, the fused RHA was then mixed with aqueous NaOH solution at different hydrothermal temperatures of 25, 40, or 105 °C, respectively, to extract silica from fused RHA. The resulting mixture was then centrifuged to separate supernatant and sediment. The silicate supernatant was then utilized as the silica precursor for the synthesis of mesoporous silica, with similar procedures described above. The synthesized mesoporous silica was denoted as MS-400(Y), where 400 denotes the fusion temperature and Y corresponds to the silicate extraction (hydrothermal) temperature of either 25, 40, or 105 °C.

For comparison purpose, the preparation of MCM-41(NaSi) and SBA-15(NaSi) from commercial silicate precursors via conventional hydrothermal process was presented as well [8]. The synthesis of MCM-41(NaSi) was carried out using pure chemicals of sodium metasilicate nanohydrate ($Na_2SiO_3{\cdot}9H_2O$) with CTAB as the structure-directing template. The molar composition of the gel mixture was 1SiO_2: 0.2 CTAB: 120 H_2O: 0.89 H_2SO_4. Mesoporous SBA-15 was synthesized using a tri-block copolymer, EO_{20}–PO_{70}–EO_{20} (Pluronic P123, BASF) as the template and sodium silicate solution (~14% NaOH, ~27% SiO_2, Aldrich) as the silica source. The molar composition of the gel mixture was 1SiO_2: 0.01 P123: 286 H_2O: 0.7 H_2SO_4.

2.2. Characterization

The specific surface area, specific pore volume and average pore diameter (BJH method) of the samples were measured by N_2 adsorption–desorption isotherms at 77 K using a surface area analyzer (Micromeritics, ASAP 2000). All the samples were degassed for 6 h at 350 °C under vacuum (10^{-6} mbar) prior to the adsorption experiments. The powder X-ray diffraction (XRD) analyses were made to reveal the crystalline structure of mesoporous materials, and the diffractograms of the mesoporous samples were recorded in the 2θ range of 2–80° in steps of 0.6 degree with a count time of 60 s at each point. The morphology of the materials was observed via the SEM (HITACHI-S4700) images. TEM images of the samples were observed with a JEOL JEM 1210 TEM instrument operated at 120 keV, prior that the samples (5–10 mg) were ultrasonicated in ethanol and dispersed on carbon film supported on copper grids (200 mesh).

2.3. Functionalization and CO_2 adsorption tests

The above mesoporous silica materials were functionalized with amine reagent of tetraethylpentaamine (TEPA) via the wet impregnation method to enhance their CO_2 capture capacity. In a typical process, all silica supports were thermally pretreated at 120 °C for 1 h. Meanwhile, TEPA was mixed with ethanol and the resulting solution was stirred for 30 min. After pretreatment, the silica adsorbents were dispersed into a flask containing TEPA solution and the mixture was then refluxed at 80 °C for 2 h. After cooling to room temperature, the obtained materials were dried at 100 °C for 2 h. The nitrogen loading of the aminated material was evaluated by a thermo-gravimetric analyzer (TGA, Netzsch TG209 F1, Germany).

To obtain the adsorption capacity and breakthrough curve of the adsorbent, CO_2 adsorption experiment was carried out by a dynamic packed column method. Prior to the adsorption, the pre-weighed adsorbent (1.0 g, 16–30 mesh powder, packing height ≈ 5 cm) was packed in a Pyrex quartz tube with an internal diameter of 0.75 cm, and placed in a temperature-controlled oven. In a typical process, the adsorbents were pretreated under a N_2 flow of 0.1 L/min at 110 °C for 1 h, and then cooled to the adsorption temperature of 75 °C. Subsequently, the gas flow was switched to 10% (v/v) CO_2 gas stream (balanced with N_2) under a flow rate of 0.1 L/min. The concentration of CO_2 was continuously measured by a CO_2 analyzer (Molecular Analytics AGM 4000 Gas Analyzer).

3. Results and discussion

3.1. Characterization of MS-X(25) and MS-400(Y) materials

The pore structures of the calcined MS-X(25) and MS-400(Y) materials are analyzed by the nitrogen adsorption–desorption measurement and the results are shown in Fig. 1a. All samples exhibited isotherms of type IV of the IUPAC classification which featuring a narrow step due to capillary condensation of nitrogen within the primary mesopores [32]. It is noted that MS-400(25) and MS-550(25) showed two uptakes of nitrogen adsorption under relative pressures of 0.25–0.40 and 0.80–1.0, respectively. Such observation revealed the presence of bimodal porosity [33] as also observed in Fig. 1b. The first hysteresis loop at p/p_o = 0.25–0.40 is related to capillary condensation of nitrogen within small intraparticle mesopores that are originated from CTAB templates. The second hysteresis loop, which lifted up sharply in the p/p_o region of 0.85–1.0, demonstrated the presence of an additional appreciable amount of secondary mesopores. As the fusion temperature further increases to 700 °C, the MS-700(25) did not show observable hysteresis loop located at relative lower pressures of 0.25–0.40, it only show the hysteresis loop in the p/p_o region of 0.80–1.0. This suggests that there is no well-defined intraparticle mesopores within MS-700(25). Furthermore, it is noteworthy that when the fusion temperature increases, the hysteresis loop and N_2 adsorption capacity at relative pressures of 0.85–1.0 decreased significantly, which reflected the decrease in the amounts of large pores of the materials.

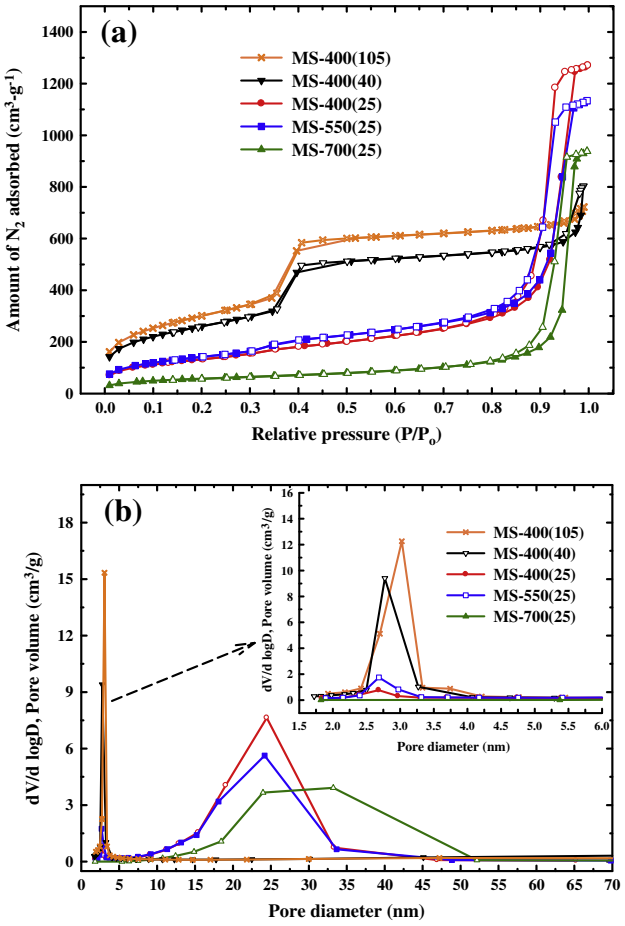

Fig. 1. (a) Nitrogen adsorption–desorption isotherms; (b) BJH pore diameter distributions of MS-400(25), MS-550(25), MS-700(25), MS-400(40) and MS-400(105).

On the other hand, as the extraction temperature increases from 25 to 40 °C and 105 °C, it is seen for MS-400(40) and MS-400(105) materials that the capillary condensation step at relative lower pressures of 0.25–0.40 with type H1 hysteresis loop became more pronounced, along with increased adsorption volume. Such phenomenon revealed the enhanced uniformity of cylindrical pore channels with higher specific surface area that were templated by CTAB [34]. Meanwhile, the hysteresis loop and adsorption capacity at relative pressures of 0.80–1.0 diminished gradually, which reflected the decrease in the amounts of large pores of the materials.

The pore size distributions of the RHA-derived MS-X(25) and MS-400(Y) samples were estimated from the BJH method with results shown in Fig. 1b. It can be seen that only MS-400(25) and MS-550(25) displayed bimodal mesopore structure consisting of small mesopores at ca. 2.7 nm as well as large mesopores at 10–50 nm. This is probably due to the presence of large inter-particle mesopores, which are derived from the aggregated silica particles. But when fusion temperature increases to 700 °C, the MS-700(25) exhibited only a broad pore size distribution at 10–50 nm. On the other hand, when the extraction temperatures were 40 and 105 °C (MS-400(40) and MS-400(105)), there appears to have only one pore size distribution at small pore range (2.7–3.0 nm) as observed in Fig. 1b.

The structural parameters of BET specific surface area (S_{BET}), total pore volume (V_{pore}) and average pore diameter (D_{pore}) as derived from nitrogen adsorption–desorption measurements are summarized in Table 1. It is seen that the MS-X(25) materials possessed mesoporous structure with specific surface area (S_{BET}) in the range of 211–518 m^2/g. The specific surface area was slightly increased with increasing fusion temperature from 400 °C to 550 °C. However, the surface area decreased drastically as fusion temperature was increased further to 700 °C. The decrease in surface area could be associated with the extensive growth and aggregation between the individual silica particles, resulting in the lower surface area of the materials. On the other hand, it is noteworthy that the specific surface areas of the MS-400(X) samples is enhanced significantly from 484 m^2/g to 945 and 1063 m^2/g as the extraction temperature increases from 25 °C to 40 °C and 105 °C.

The crystalline structure of MS-X(25) and MS-400(X) samples were revealed by the powder XRD patterns as shown in Fig. 2. It is observed from Fig. 2a that all MS-X(25) samples exhibited one main intensive peak at 2θ of ca. 22°, which are characteristic of silica materials with randomly arranged pore structures [24,35]. When the extraction temperature was increased from 25 °C to 40 and 105 °C, it is seen from Fig. 2b that one main intensive (100) peak at 2θ of ca. 2° and another peak (110) diffraction peak at 2θ of ca. 3.7° appeared for MS-400(40) and MS-400(105), indicating the presence of hexagonal array and one-dimensional channel structure [36]. With a further increase of extraction temperature to 105 °C, the (100) peak shifted slightly to a higher angle, which

Table 1
Structural parameters of the silica materials.

Sample name	[a]Fusion temperature (°C)	[b]Extraction temperature (°C)	S_{BET} (m^2/g)	d_{BJH} (nm)	V_p (cm^3/g)
MS-400(25)	400	25	484	14.4	1.92
MS-550(25)	550	25	518	11.8	1.71
MS-700(25)	700	25	211	25.8	1.36
MS-400 (40)	400	40	945	4.4	0.97
MS-400 (105)	400	105	1063	3.4	1.00
MCM-41(NaSi)	–	–	1064	3.0	1.00
SBA-15(NaSi)	–	–	801	6.5	1.02

[a] Fusion temperature of raw rice husk.
[b] Extraction (hydrothermal) temperature for the extraction of silicate from pre-heated rice husk ash.

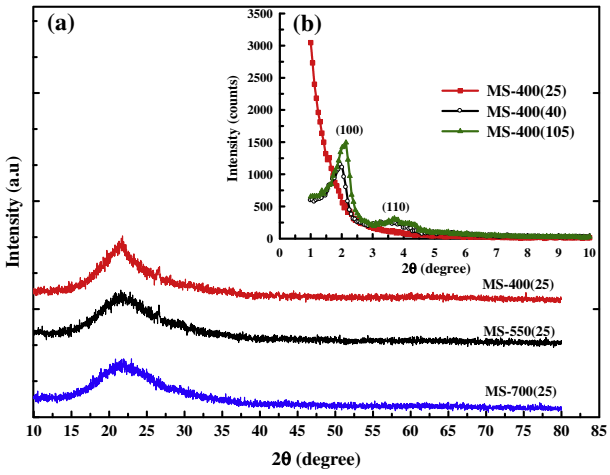

Fig. 2. XRD patterns of MS-400(25), MS-550(25), MS-700(25), MS-400(40) and MS-400(105).

could be associated with the slightly diminished pore diameter of MS-400(105). This is in line with nitrogen physisorption results in which MS-400(40) shows larger pore diameter than that of MS-400(105) as showed in Table 1.

The morphologies of MS-400(25) and MS-400(105) samples are revealed by the SEM images, as illustrated in Fig. 3a and b. It can be clearly observed that aggregated nanoparticles with ca. 50–100 nm particle size are formed for the MS-400(25); on the contrary, MS-400(105) is mainly consisted of tubular and irregular shapes. The textural mesostructure of the MS-400(25) and MS-400(105) are further characterized by TEM images and the results are shown in Fig. 3c and d. The TEM image of MS-400(25) material consists of both small and large mesopores (Fig. 3c). The small mesopores could be ascribed to the mesopores templated by the CTAB surfactants, while the large mesopores could be related to the pores interconnected by the formed silica nanoparticles. On the other hand, MS-400(105) material (Fig. 3d) clearly shows a long range hexagonal array of mesopores. The mesostrucure is composed of unidirectional pore orientation within tubular particles, which is

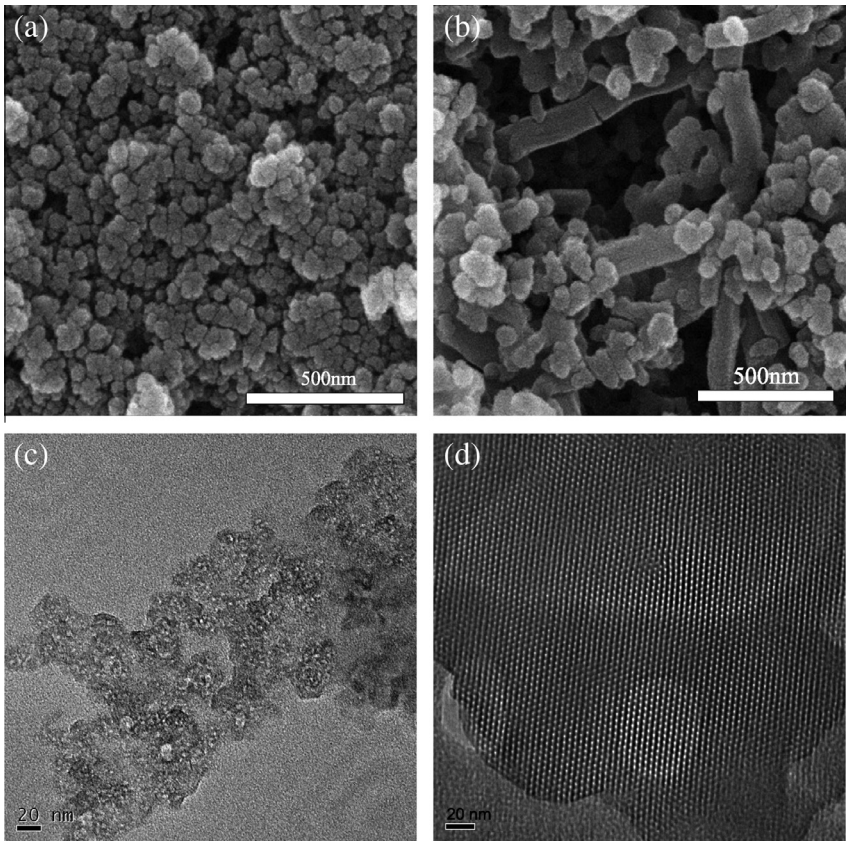

Fig. 3. SEM images of mesoporous silica materials: (a) MS-400(25), (b) MS-400(105); and TEM images of mesoporous silica materials: (c) MS-400(25) and (d) MS-400(105).

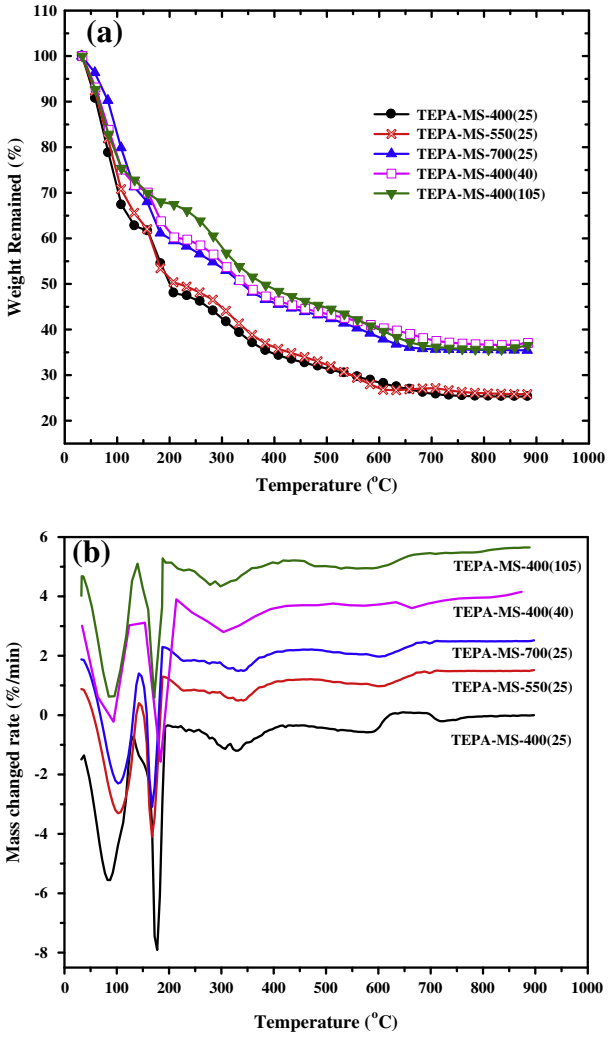

Fig. 4. (a) TG profiles; (b) DTG profiles of 50 wt.% TEPA-impregnated mesoporous silica adsorbents.

similar with the characteristic of MCM-41 synthesized via conventional aqueous route [36].

3.2. CO_2 adsorption over TEPA-impregnated mesoporous silica-based adsorbents

The nitrogen loadings on 50 wt.% TEPA-impregnated adsorbents were evaluated by the thermo-gravimetric analyses (TG/DTG) with results shown in Fig. 4a and b. All aminated adsorbents show a broad temperature range of their weight losses as seen from Fig. 4a. The first weight loss region at <120 °C is mainly from the evaporation of the physically adsorbed water on the surface of the adsorbents. The weight losses at second regions of around 120–200 °C are very significant. It is observed from the DTG profile (Fig. 4b) that the maximum mass change rates appeared at around 170–200 °C, and this is mainly attributed to Hofmann elimination of trimethylamine in TEPA-impregnated adsorbents [37,38]. The third weight loss regions (200–700 °C) are due to the carbon chain ($C–H_2$) decomposition by oxidation processes [18].

The TEPA contents were calculated based on the mass losses observed in the temperature range of 120–700 °C and the results were expressed as N loading and summarized in Table 2. The N loadings were calculated to be 9.85, 10.39, 10.13, 9.17 and 9.86 mmol of nitrogen adsorption sites per gram of silica, respectively, for TEPA-MS-400(25), TEPA-MS-550(25), TEPA-MS-700(25), TEPA-MS-400(40) and TEPA-MS-400(105). It can be observed that all aminated sorbents exhibited similar S_{BET} and N loadings after 50 wt.% TEPA impregnation.

Fig. 5a displays the breakthrough curves of 10% CO_2 adsorption on TEPA-impregnated MS materials at 75 °C via the packed column reactor. For comparison basis, mesoporous MCM-41(NaSi) and SBA-15(NaSi) silica materials synthesized from commercial sodium silicate solution via conventional hydrothermal process were also used as supports for their CO_2 adsorption performance. Their structural properties including specific surface area, pore size and total pore volume are summarized in Table 1. It is seen that the CO_2 gas could be effectively adsorbed on all adsorbents with capture efficiency of near 100% at the beginning. But the CO_2 concentration using TEPA-SBA-15(NaSi) raised first ($C_{eff}/C_{in} > 0.0$), while the TEPA-MCM-41(NaSi) reached the saturated point ($C_{eff}/C_{in} = 1.0$) first. On the other hand, both the breakthrough time ($C_{eff}/C_{in} = 0.05$) and the saturated time ($C_{eff}/C_{in} = 1.0$) of the TEPA-MS-400(25) adsorbent were the longest among all tested adsorbents. This indicated that TEPA-MS-400(25) is the best CO_2 adsorbent among all tested materials.

Fig. 5b shows the saturated adsorption capacities of all 50 wt.% TEPA-impregnated adsorbents. The CO_2 adsorption capacities of all tested adsorbents were in the range of 113–155 mg/g-adsorbent which followed the order of TEPA-MS-400(25) > TEPA-MS-550(25) > TEPA-MS-700(25) > TEPA-MS-400(40) ≈ TEPA-MS-400(105) ≈ TEPA-MCM-41(NaSi) ≈ TEPA-SBA-15(NaSi). There are many parameters determining the sorbent capacity, e.g. support textural property and surface density of amines. It is generally accepted that supports with high-surface-area are beneficial for a better dispersion of amines on the support and high sorbent capacity [10,39]. As observed from Tables 1 and 2, however, there is no relationship between S_{BET} and CO_2 uptake. It is well-known that the adsorption of CO_2 over TEPA-impregnated adsorbents was carried out between the acidic CO_2 molecules and the basic amino groups within TEPA molecules. Generally, the following chemical reactions are expected to take place when CO_2 molecules react with TEPA under anhydrous conditions [14]:

Table 2
Structural properties, nitrogen loading and CO_2 uptakes of sorbents after impregnated with 50 wt.% TEPA.

Sample name	S_{BET} (m^2/g)	V_p (cm^3/g)	[a]N loading (mmol/g)	[b]N surface density (N atom/nm^2)	CO_2 capacity (mg/g) at 10% CO_2, 75 °C	Amine efficiency CO_2/2N (mmol/mmol)
TEPA-MS-400(25)	33	0.30	9.85	12.25	155 ± 5	0.72
TEPA-MS-550(25)	31	0.25	10.39	12.07	141 ± 4	0.62
TEPA-MS-700(25)	28	0.19	10.13	28.90	124 ± 6	0.56
TEPA-MS-400(40)	30	0.13	9.17	5.85	116 ± 3	0.58
TEPA-MS-400(105)	40	0.15	9.86	5.59	113 ± 3	0.52
TEPA-MCM-41(NaSi)	53	0.15	11.28	6.38	114 ± 3	0.46
TEPA-SBA-15(NaSi)	40	0.11	10.61	7.97	114 ± 3	0.48

[a] Calculated based on the mass loss in the temperature of 120–700 °C.
[b] Calculated based on the amount of nitrogen per 1 nm^2 of the parent mesoporous silica support.

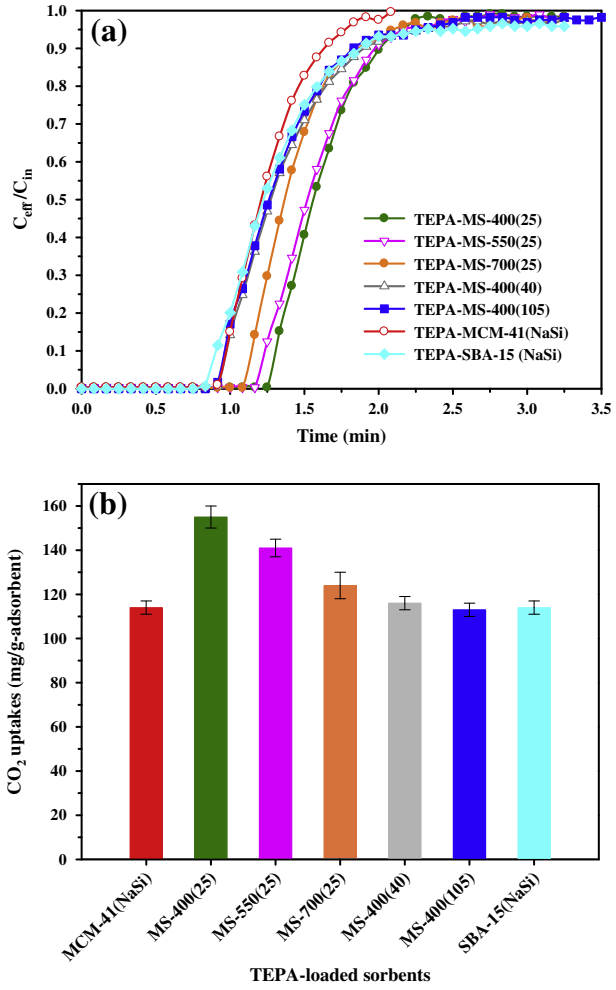

Fig. 5. (a) CO_2 breakthrough curves; (b) CO_2 uptakes of 50 wt.% TEPA-impregnated sorbents as tested under 10% CO_2 at 75 °C.

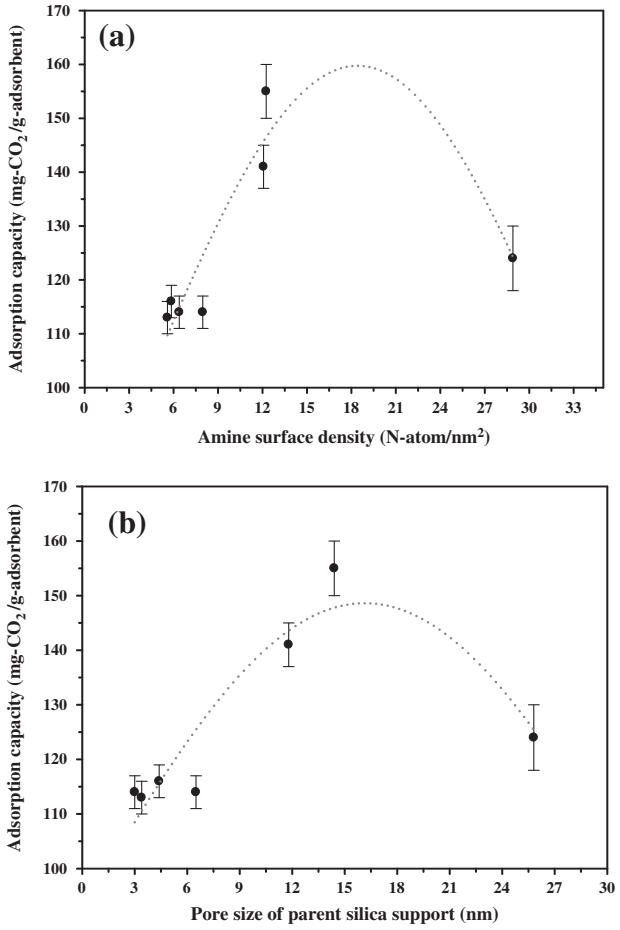

Fig. 6. (a) Relationship between the amine surface density of the parent mesoporous supports and their CO_2 uptakes; (b) relationship between the pore diameter of the parent mesoporous supports and their CO_2 uptakes. Sorbents: 50 wt.% TEPA-impregnated silicas; adsorption temperature: 75 °C; CO_2 inlet concentration: 10%.

$$CO_2 + 2RNH_2 \rightarrow RNHCOO^- + RNH_3^+ \quad (1)$$

$$CO_2 + 2R_1R_2NH \rightarrow R_1NHCOO^- + R_2NH_2 + (\text{or}\, R_2NCOO^- + R_1NH_2^+) \quad (2)$$

$$CO_2 + R_2NH + RNH_2 \rightarrow R_2NCOO^- + RNH_3^+ (\text{or}\, RNHCOO^- + R_2NH_2^+) \quad (3)$$

In the absence of moisture, one mole of CO_2 is adsorbed on TEPA-impregnated adsorbents through formation of carbamate ion, where two moles of nitrogen atoms in the amine are consumed. In an earlier study, CO_2 adsorption capacity was demonstrated to be strongly dependent on the surface density of amine species [40]. They found that densely amino groups are more effective as adsorption sites than those isolated on bare silica supports. Liu et al. [41] also concluded that the key parameter influencing the CO_2 adsorption is not surface area but might be the surface density of amines on the sorbents.

The influence of surface density of amines on the sorbent capacity is plotted in Fig. 6a. It is seen that the sorbent capacity increased linearly with increasing surface density of amine in the range of 5–13 N-atom/nm^2. This may reveal that higher surface density of amine groups is beneficial for enhancing the CO_2 adsorption performance. This result is similar with a recent work of Liu et al. [42], who conducted the CO_2 adsorption over amine-impregnated mesoporous silica materials and found that the CO_2 adsorption is in proportion to the surface density of amine groups in the range of 4–23 N-atom/nm^2. However, it is noted from both Fig. 6a and Table 2 that as N surface density increases from 5.59 N-atom/nm^2 to 7.97 N-atom/nm^2, the CO_2 capacity was almost unchanged. While as further increasing the surface density of amine groups to 28.9 N-atom/nm^2 (TEPA-MS-700(25) sorbent), a drastic decline in the CO_2 adsorption capacity was observed (124 mg/g-adsorbent). The above observations may reveal that the N surface density is not the only parameter affecting CO_2 adsorption performance in these aminated adsorbents. The pore texture of the mesoporous silica support may significantly influence the dispersion and accessibility of the impregnated amines, and thus affect the CO_2 uptake.

In addition to amine surface density, structural properties of silica support such as pore size and pore volume might also be influencing factors on CO_2 adsorption. Zeleňák et al. [43] and Son et al. [44] found that the enlargement of pore diameter of the silica support would enhance the CO_2 adsorption performance. They concluded that the amine was introduced into the pore channels more easily as the pore diameter of the mesoporous silica support increases. As seen from Fig. 6b, the sorbent performance increased linearly with increasing pore size in the range of 3.0–14.4 nm. However, the adsorption capacity decreased drastically for the largest pore size of 25.8 nm (TEPA-MS-700(25) sorbent). The results shown in Fig. 6a and b may suggest that although higher amine surface density and larger pore size of the silica support could enhance the CO_2 adsorption, their positive influence is limited to a certain degree.

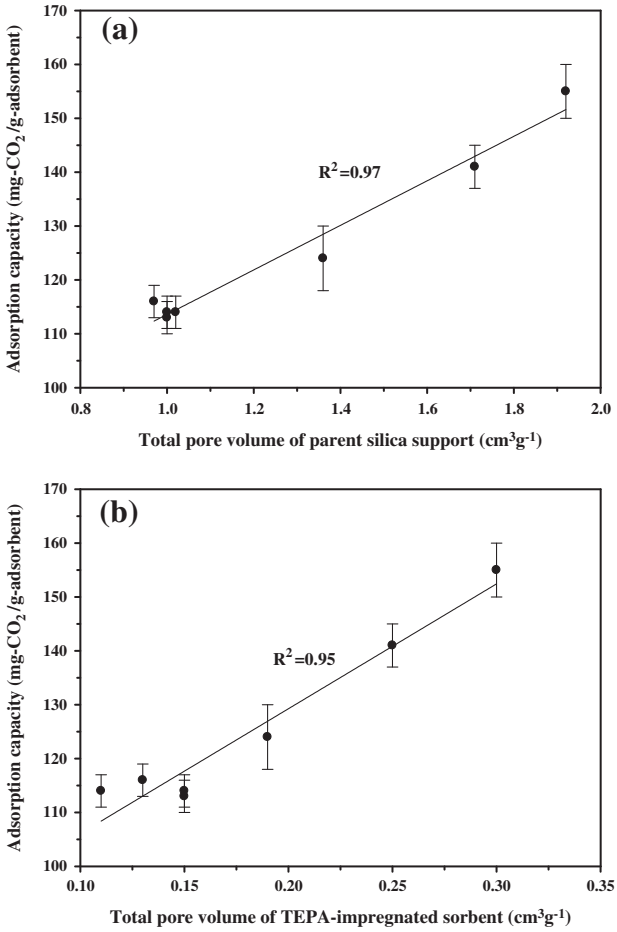

Fig. 7. Relationship between the total pore volume of mesoporous silicas and their CO_2 uptakes as expressed based on (a) the pore volume of parent mesoporous supports; and (b) the remaining pore volume of TEPA-impregnated mesoporous adsorbents. Sorbents: 50 wt.% TEPA-impregnated silicas; adsorption temperature: 75 °C; CO_2 inlet concentration: 10%.

The sorbent capacity, on the other hand, correlated well to the total pore volume of the parent silica support as observed in Fig. 7a. A high correlation coefficient of $R^2 = 0.97$ is observed between the total pore volume of the parent silica supports and the CO_2 capacity (Fig. 7a). This is in line with the work by Yan et al. [45], who reported that the total pore volume of the parent mesoporous SBA-15 support played a predominated role in CO_2 adsorption rather than pore diameter. Yan et al. [45] conducted CO_2 adsorption tests over SBA-15 based materials of similar pore architectures, while the supports employed in this work including different pore architectures and morphologies of MCM-41(NaSi), SBA-15(NaSi), MS-X(25) and MS-400(Y). Therefore, it might be deduced that the sorbent performance is well correlated to the total pore volume of the support, regardless of their structural properties.

Furthermore, the total pore volume of sorbents after impregnated with 50 wt.% TEPA was also measured to study on their correlation with the CO_2 sorbent capacity and the result is shown in Fig. 7b. It is interesting to see that a high correlation ($R^2 = 0.95$) still appeared between the CO_2 capacity and total pore volume of aminated sorbents. This clearly indicates that the more residual space left inside the pores of the silica support after loading with the same amount of amine, the more efficient contact between the CO_2 molecules and the impregnated amines. This prevents the blockage of pores from effective adsorption and thus favors higher sorbent capacity and amine utilization.

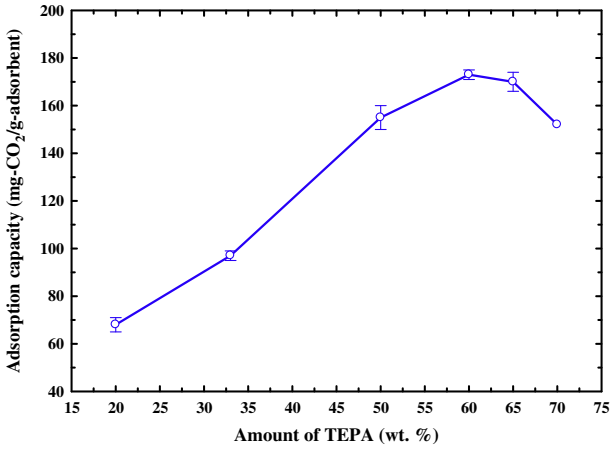

Fig. 8. Effect of amine loading on sorbent capacity of TEPA-MS-400(25). Adsorption temperature: 75 °C; CO_2 test concentration: 10%.

To further determine the optimal amine loading on the silica support for CO_2 adsorption and the relationship between the CO_2 capacity and amine loadings, MS-400(25) support impregnated with various TEPA contents was used for CO_2 adsorption. Fig. 8 shows the saturated adsorption capacities and total pore volume as a function of TEPA loaded content for the MS-400(25) sorbents, and their structural properties are summarized in Table 3. It is seen from Table 3 that both the surface area and total pore volume decrease significantly with increasing TEPA loading amount in the range of 20–70 wt.%. And a linear increase in adsorption capacity with increasing TEPA loading in the range of 20–60 wt.% is observed. The highest capacity for the MS-400(25) sample was 173 mg/g-adsorbent at 60 wt.% TEPA as observed in Fig. 8. However, a further increase in the TEPA content to 70 wt.% leads to a decrease in the adsorption capacity of MS-400(25) sorbent. The density of TEPA is 0.99 cm^3/g and the total pore volume of MS-400(25) is 1.92 cm^3/g. Thus the maximum theoretical TEPA amounts loaded inside the pore channels is calculated to be 66%. When the TEPA content is beyond 65 wt.%, the pores of MS-400(25) were nearly filled. Therefore, this may easily result in the blockage of effective adsorption sites within the pores, leading to the decrease in adsorption capacity. It is also noteworthy from Table 3 that the total pore volume of 65 wt.% TEPA-impregnated MS-400(25) is 0.15 cm^3/g, which is similar to those of MS-400(105), MCM-41(NaSi) and SBA-15(NaSi) sorbents at 50 wt.% TEPA (Table 2), but it has a much higher CO_2 uptakes than these three sorbents. This clearly implies that larger pore volume is beneficial for accommodating and dispersing more TEPA molecules inside the pore channels without pore blockage. Taking into account the above structure-sorbent capacity relationship, it may conclude that the mesoporous silica support with high specific surface area and uniform mesostructures are not key parameters affecting the CO_2 sorbent performance. The amine surface density, pore diameter and total pore volume of the support seem to largely

Table 3
Effect of TEPA amounts on CO_2 capture over MS-400(25) sorbent.

Sample name	TEPA loading (wt.%)	S_{BET} (m^2/g)	V_p (cm^3/g)	N loading (mmol/g)
TEPA-MS-400(25)	20	217	1.2	5.45
	33	190	0.96	6.96
	50	33	0.30	9.85
	60	22	0.22	13.92
	65	15	0.15	15.14
	70	9	0.09	16.72

Table 4
Comparison of TEPA-related sorbents for CO_2 capture.

Support	Precursors	Test conditions	TEPA amount (wt.%)	Capacity (mg/g)	Reference
As-prepared MSU-1	Sodium silicate + alcohol polyoxyethylene ether	10% CO_2, 75 °C	50	172	[14]
KIT-6	TEOS + P123	10% CO_2, 75 °C	50	128	[46]
SBA-15	TEOS + P123	10% CO_2, 75 °C	60	153	[47]
Silica aerogels	–	10% CO_2, 75 °C	80	154	[48]
MCFs	TEOS + P123 + TMB + NH_4F	10% CO_2, 75 °C	70	191	[38]
MS-400(25)	Waste derived silica (RHA) + CTAB	10% CO_2, 75 °C	60	173	This study

influence the adsorption capacity, and among which the total pore volume of the mesoporous silica support appears to play a dominant role in determining the CO_2 adsorption performance.

The capture of CO_2 has been studied over various sorbents during past years. Table 4 summarizes the comparison of TEPA-related sorbents for CO_2 capture. All supports listed in Table 4 cited from literature were manufactured from pure chemical sources of silica [14,38,46–48]. Among them the TEPA-impregnated MCFs exhibited the highest CO_2 adsorption capacity of 191 mg/g, which can be considered as high efficient adsorbents for CO_2 capture. However, both of the cost and environmental hazard for the production of MCFs materials are high because it requires the use of pure silica chemicals and pore expander as well. On the other hand, the TEPA-impregnated MS-400(25), which CO_2 adsorption capacity (173 mg/g adsorbent) was only second to and slightly less than that of TEPA-MCFs. The MS-400(25) material can be facilely prepared using rice husk wastes as silica precursor through a simple temperature-controlled method. The MS-400(25) with large pore size and large pore volume was obtained under mild conditions without the use of expensive pore expanders and/or post-pore-expansion treatments, which can reduce the cost and significantly simplify the scale-up synthesis.

4. Conclusions

A simple method for preparing silica support materials with large pore size and large pore volume has been demonstrated in this study using rice husk waste as the silica source. By altering the fusion and hydrothermal temperatures, the silica materials with adjustable mesoporosities can be easily obtained. The nitrogen physisorption measurement, SEM and TEM results suggested that the obtained MS-400(25) exhibits pore volume (1.92 $cm^3\ g^{-1}$) larger than that of the MCM-41 material, and bimodal mesopores (2.7 and 14.4 nm) which make it a desirable support material of amine immobilization for CO_2 capture. The TEPA-impregnated MS-400(25) adsorbent appeared to be more efficient and lower cost than other supports reported in the literature, it achieved a good CO_2 adsorption capacity of 173 mg/g adsorbent under 10% CO_2 at 75 °C. The above results might suggest that MS-400(25) could be considered as a potential support of adsorbent in terms of CO_2 adsorption, which performs several advantages of simple and cost-effective synthesis as well as superior adsorption performance.

Acknowledgment

The authors gratefully acknowledge the financial support from the National Science Council of the Republic of China through Grant No.: NSC 102-2221-E-009-009-MY1.

References

[1] C. Pevida, M.G. Plaza, B. Arias, J. Fermoso, F. Rubiera, J.J. Pis, Surface modification of activated carbons for CO_2 capture, Appl. Surf. Sci. 254 (2008) 7165–7172.
[2] L.-Y. Lin, H. Bai, Continuous generation of mesoporous silica particles via the use of sodium metasilicate precursor and their potential for CO_2 capture, Micropor. Mesopor. Mater. 136 (2010) 25–32.
[3] Y.G. Ko, H.J. Lee, H.C. Oh, U.S. Choi, Amines immobilized double-walled silica nanotubes for CO_2 capture, J. Hazard. Mater. 250–251 (2013) 53–60.
[4] K. Ahmad, O. Mowla, E.M. Kennedy, B.Z. Dlugogorski, J.C. Mackie, M. Stockenhuber, A melamine-modified β-zeolite with enhanced CO_2 capture properties, Energy Technol. 1 (2013) 345–349.
[5] A.A. Olajire, CO_2 capture and separation technologies for end-of-pipe applications – a review, Energy 35 (2010) 2610–2628.
[6] A. Samanta, A. Zhao, G.K.H. Shimizu, P. Sarkar, R. Gupta, Post-combustion CO_2 capture using solid sorbents: a review, Ind. Eng. Chem. Res. 51 (2012) 1438–1463.
[7] L.-Y. Lin, H. Bai, Aerosol processing of low-cost mesoporous silica spherical particles from photonic industrial waste powder for CO_2 capture, Chem. Eng. J. 197 (2012) 215–222.
[8] L.-Y. Lin, H. Bai, Facile and surfactant-free route to mesoporous silica-based adsorbents from TFT-LCD industrial waste powder for CO_2 capture, Micropor. Mesopor. Mater. 170 (2013) 266–273.
[9] A. Sayari, Y. Belmabkhout, R. Serna-Guerrero, Flue gas treatment via CO_2 adsorption, Chem. Eng. J. 171 (2011) 760–774.
[10] X. Xu, C. Song, J.M. Andrésen, B.G. Miller, A.W. Scaroni, Preparation and characterization of novel CO_2 "molecular basket" adsorbents based on polymer-modified mesoporous molecular sieve MCM-41, Micropor. Mesopor. Mater. 62 (2003) 29–45.
[11] R. Sanz, G. Calleja, A. Arencibia, E.S. Sanz-Pérez, Amino functionalized mesostructured SBA-15 silica for CO_2 capture: exploring the relation between the adsorption capacity and the distribution of amino groups by TEM, Micropor. Mesopor. Mater. 158 (2012) 309–317.
[12] C. Chen, W.-J. Son, K.-S. You, J.-W. Ahn, W.-S. Ahn, Carbon dioxide capture using amine-impregnated HMS having textural mesoporosity, Chem. Eng. J. 161 (2010) 46–52.
[13] Y. Liu, Q. Ye, M. Shen, J. Shi, J. Chen, H. Pan, Y. Shi, Carbon dioxide capture by functionalized solid amine sorbents with simulated flue gas conditions, Environ. Sci. Technol. 45 (2011) 5710–5716.
[14] X. Wang, H. Li, H. Liu, X. Hou, AS-synthesized mesoporous silica MSU-1 modified with tetraethylenepentamine for CO_2 adsorption, Micropor. Mesopor. Mater. 142 (2011) 564–569.
[15] H.C. Wang, C. Lu, H. Bai, J.F. Hwang, H.H. Lee, W. Chen, Y. Kang, S.-T. Chen, F. Su, S.-C. Kuo, F.-C. Hu, Pilot-scale production of mesoporous silica-based adsorbent for CO_2 capture, Appl. Surf. Sci. 258 (2012) 6943–6951.
[16] X. Yan, L. Zhang, Y. Zhang, K. Qiao, Z. Yan, S. Komarneni, Amine-modified mesocellular silica foams for CO_2 capture, Chem. Eng. J. 168 (2011) 918–924.
[17] C. Chen, K.-S. You, J.-W. Ahn, W.-S. Ahn, Synthesis of mesoporous silica from bottom ash and its application for CO_2 sorption, Korean J. Chem. Eng. 27 (2010) 1010–1014.
[18] X. Zhang, X. Zheng, S. Zhang, B. Zhao, W. Wu, AM-TEPA impregnated disordered mesoporous silica as CO_2 capture adsorbent for balanced adsorption–desorption properties, Ind. Eng. Chem. Res. 51 (2012) 15163–15169.
[19] G. Qi, L. Fu, B.H. Choi, E.P. Giannelis, Efficient CO_2 sorbents based on silica foam with ultra-large mesopores, Energy Environ. Sci. 5 (2012) 7368–7375.
[20] L. Estevez, R. Dua, N. Bhandari, A. Ramanujapuram, P. Wang, E.P. Giannelis, A facile approach for the synthesis of monolithic hierarchical porous carbons – high performance materials for amine based CO_2 capture and supercapacitor electrode, Energy Environ. Sci. 6 (2013) 1785–1790.
[21] C. Chen, S.-T. Yang, W.-S. Ahn, R. Ryoo, Amine-impregnated silica monolith with a hierarchical pore structure: enhancement of CO_2 capture capacity, Chem. Commun. (2009) 3627–3629.
[22] T.-H. Liou, A green route to preparation of MCM-41 silicas with well-ordered mesostructure controlled in acidic and alkaline environments, Chem. Eng. J. 171 (2011) 1458–1468.
[23] V. Meynen, P. Cool, E.F. Vansant, Verified syntheses of mesoporous materials, Micropor. Mesopor. Mater. 125 (2009) 170–223.
[24] D. An, Y. Guo, Y. Zhu, Z. Wang, A green route to preparation of silica powders with rice husk ash and waste gas, Chem. Eng. J. 162 (2010) 509–514.
[25] X. Ma, B. Zhou, W. Gao, Y. Qu, L. Wang, Z. Wang, Y. Zhu, A recyclable method for production of pure silica from rice hull ash, Powder Technol. 217 (2012) 497–501.
[26] A. Olea, E.S. Sanz-Pérez, A. Arencibia, R. Sanz, G. Calleja, Amino-functionalized pore-expanded SBA-15 for CO_2 adsorption, Adsorption 19 (2013) 589–600.
[27] A. Heydari-Gorji, Y. Belmabkhout, A. Sayari, Polyethylenimine-impregnated mesoporous silica: effect of amine loading and surface alkyl chains on CO_2 adsorption, Langmuir 27 (2011) 12411–12416.

[28] C. Gérardin, J. Reboul, M. Bonne, B. Lebeau, Ecodesign of ordered mesoporous silica materials, Chem. Soc. Rev. 42 (2013) 4217–4255.
[29] A. Kaithwas, M. Prasad, A. Kulshreshtha, S. Verma, Industrial wastes derived solid adsorbents for CO_2 capture: a mini review, Chem. Eng. Res. Des. 90 (2012) 1632–1641.
[30] M. Olivares-Marín, M.M. Maroto-Valer, Development of adsorbents for CO_2 capture from waste materials: a review, Greenh. Gases Sci. Technol. 2 (2012) 20–35.
[31] T. Witoon, Polyethyleneimine-loaded bimodal porous silica as low-cost and high-capacity sorbent for CO_2 capture, Mater. Chem. Phys. 137 (2012) 235–245.
[32] J. Yu, Y. Le, B. Cheng, Fabrication and CO_2 adsorption performance of bimodal porous silica hollow spheres with amine-modified surfaces, RSC Adv. 2 (2012) 6784–6791.
[33] Q. Wu, F. Zhang, J. Yang, Q. Li, B. Tu, D. Zhao, Synthesis of ordered mesoporous alumina with large pore sizes and hierarchical structure, Micropor. Mesopor. Mater. 143 (2011) 406–412.
[34] C.T. Kresge, M.E. Leonowicz, W.J. Roth, J.C. Vartuli, J.S. Beck, Ordered mesoporous molecular sieves synthesized by a liquid-crystal template mechanism, Nature 359 (1992) 710–712.
[35] F. Adam, T.-S. Chew, J. Andas, A simple template-free sol–gel synthesis of spherical nanosilica from agricultural biomass, J. Sol–Gel Sci. Technol. 59 (2011) 580–583.
[36] C. Hung, H. Bai, M. Karthik, Ordered mesoporous silica particles and Si-MCM-41 for the adsorption of acetone: a comparative study, Sep. Purif. Technol. 64 (2009) 265–272.
[37] L.-Y. Lin, J.-T. Kuo, H. Bai, Silica materials recovered from photonic industrial waste powder: its extraction, modification, characterization and application, J. Hazard. Mater. 192 (2011) 255–262.
[38] X. Feng, G. Hu, X. Hu, G. Xie, Y. Xie, J. Lu, M. Luo, Tetraethylenepentamine-modified siliceous mesocellular foam (MCF) for CO_2 capture, Ind. Eng. Chem. Res. 52 (2013) 4221–4228.
[39] X. Xu, C. Song, J.M. Andresen, B.G. Miller, A.W. Scaroni, Novel polyethylenimine-modified mesoporous molecular sieve of MCM-41 type as high-capacity adsorbent for CO_2 capture, Energy Fuels 16 (2002) 1463–1469.
[40] N. Hiyoshi, K. Yogo, T. Yashima, Adsorption characteristics of carbon dioxide on organically functionalized SBA-15, Micropor. Mesopor. Mater. 84 (2005) 357–365.
[41] S.-H. Liu, C.-H. Wu, H.-K. Lee, S.-B. Liu, Highly stable amine-modified mesoporous silica materials for efficient CO_2 capture, Top. Catal. 53 (2010) 210–217.
[42] S.-H. Liu, Y.-C. Lin, Y.-C. Chien, H.-R. Hyu, Adsorption of CO_2 from flue gas streams by a highly efficient and stable aminosilica adsorbent, J. Air Waste Manage. Assoc. 61 (2011) 226–233.
[43] V. Zeleňák, M. Badaničová, D. Halamová, J. Čejka, A. Zukal, N. Murafa, G. Goerigk, Amine-modified ordered mesoporous silica: effect of pore size on carbon dioxide capture, Chem. Eng. J. 144 (2008) 336–342.
[44] W.-J. Son, J.-S. Choi, W.-S. Ahn, Adsorptive removal of carbon dioxide using polyethyleneimine-loaded mesoporous silica materials, Micropor. Mesopor. Mater. 113 (2008) 31–40.
[45] X. Yan, L. Zhang, Y. Zhang, G. Yang, Z. Yan, Amine-modified SBA-15: effect of pore structure on the performance for CO_2 capture, Ind. Eng. Chem. Res. 50 (2011) 3220–3226.
[46] Y. Liu, J. Shi, J. Chen, Q. Ye, H. Pan, Z. Shao, Y. Shi, Dynamic performance of CO_2 adsorption with tetraethylenepentamine-loaded KIT-6, Micropor. Mesopor. Mater. 134 (2010) 16–21.
[47] A. Zhao, A. Samanta, P. Sarkar, R. Gupta, Carbon dioxide adsorption on amine-impregnated mesoporous SBA-15 sorbents: experimental and kinetics study, Ind. Eng. Chem. Res. 52 (2013) 6480–6491.
[48] N. Linneen, R. Pfeffer, Y.S. Lin, CO_2 capture using particulate silica aerogel immobilized with tetraethylenepentamine, Micropor. Mesopor. Mater. 176 (2013) 123–131.